Chapter 4

Results and Discussion

4.1 Raw materials characterization

4.1.1 Phase analysis

The phases of all as-received raw materials were identified by XRD. As compared to JCPDS files (Appendix A), the XRD results of almost all oxides and carbonate showed their own single phase as illustrated in Fig.4.1. The XRD patterns of $SrCO_3$, Mn_2O_3, Co_3O_4 and Fe_2O_3 corresponded to the JCPDS files no.05-0418, 24-0508, 43-1003 and 33-0664, respectively. Exceptionally, the XRD pattern of La_2O_3 raw material as compared to a standard file showed small peaks at 2θ 27.32°, 28.02° and 47.78°, corresponding to the JCPDS no.36-1481 of $La(OH)_3$. This indicated that La_2O_3 was a hygroscopic material, and hence easily absorbing moisture to form $La(OH)_3$. From this result, La_2O_3 was calcined before introduced as a raw material for sample preparation.

4.1.2 Thermal analysis of as-received La_2O_3

$La(OH)_3$ found in as-received La_2O_3 can make an error in weighing of La_2O_3 due to the difference of molecular weight, which give rise to the deviation of final compositions. In order to prepare stoichiometric composition, pure La_2O_3 is required. However, an actual content of $La(OH)_3$ was difficult to specified since it depends on moisture content, temperature and time of its storage. The calcination of as-received La_2O_3 was expected to eliminate $La(OH)_3$ phase. The appropriate calcining temperature was determined by DTA and TGA, and their results were shown in Fig.4.2. The DTA curves depicted the temperatures at which the reactions of as-received La_2O_3 occurred. The endothermic reactions took place about 344°C and 514°C. Similarly, the analysis from TGA indicated that the weight loss occurred around the same temperatures as the result from DTA, suggesting that the absorbed moisture or hydroxyl ion was removed from $La(OH)_3$. The dehydroxylation of $La(OH)_3$ produced LaO(OH) phase about 300-350°C and then La_2O_3

phase approximately at 450-470°C. These results were in good agreement with the work published by Ali et al.[21,22]. The total weight loss from this experiment was 14.5%. However, the weight loss was different at different time analysis, depending upon the amount of moisture absorbed into the material. On further heating, the weight loss insignificantly increased and the reactions seemed to complete at 750°C.

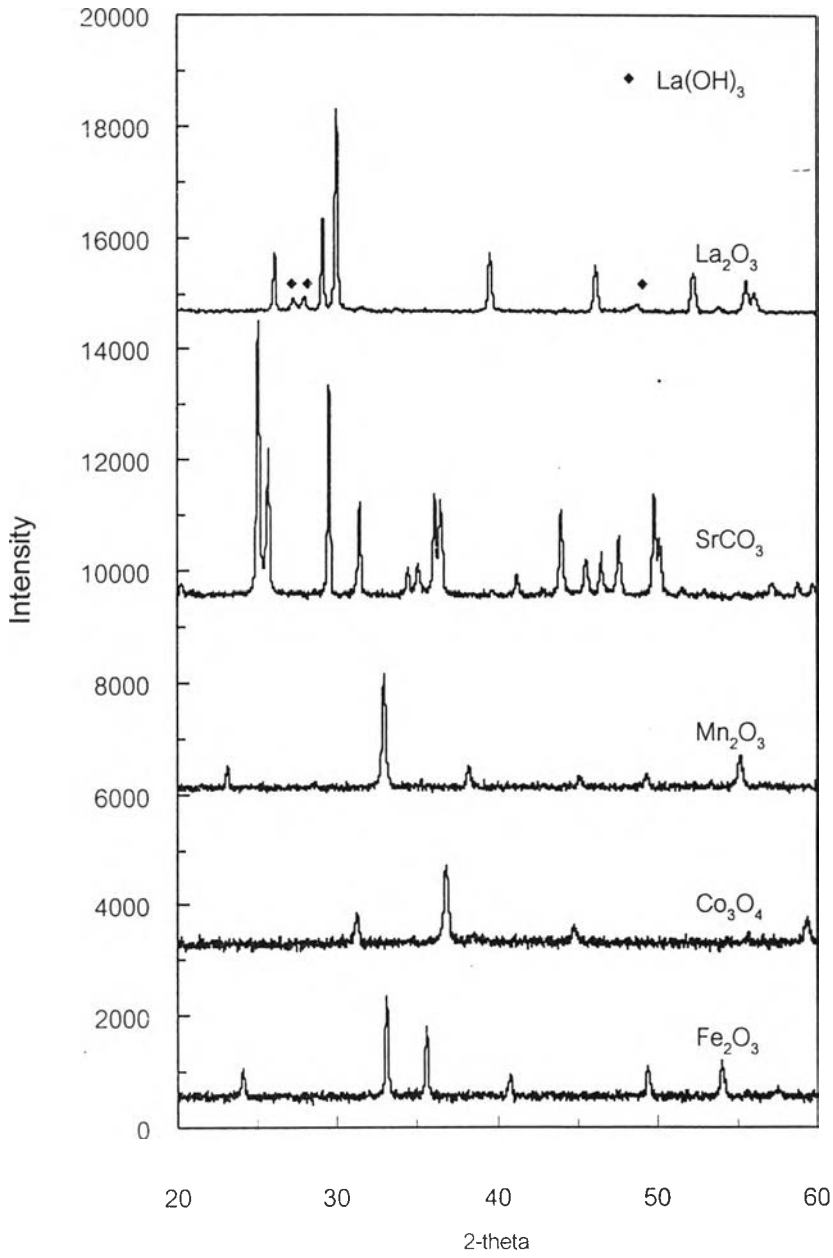

Fig.4.1 XRD patterns of received raw materials

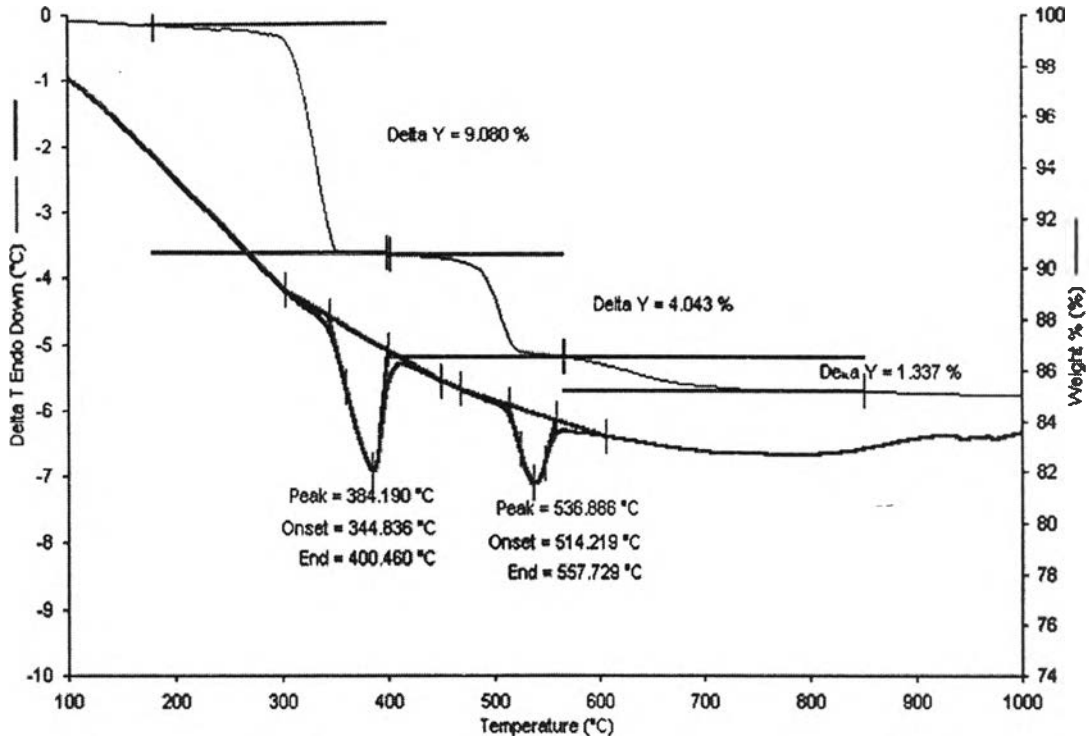

Fig.4.2 DTA and TGA traces of as-received La_2O_3

As a results of DTA and TGA, the calcining schedule of La_2O_3 as shown in Fig.4.3 was set up. In order to ensure that the calcining condition can remove hydroxyl group completely from La_2O_3 raw material, the maximum temperature was set at 1000°C. The result of XRD patterns in Fig.4.4 showed that there was no remaining $La(OH)_3$ left in La_2O_3. Therefore, the calcined La_2O_3 powder was used to prepare the stoichiometric composition in this research.

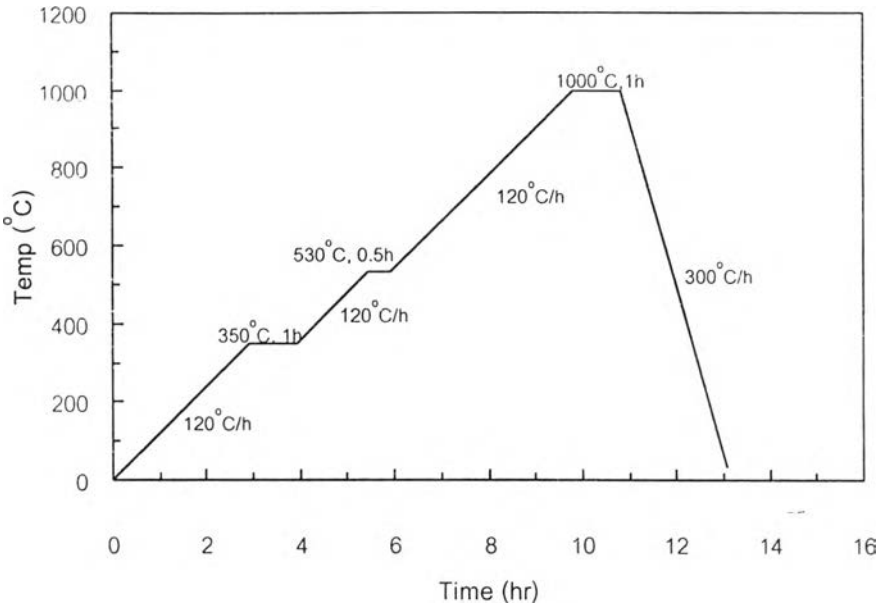

Fig.4.3 The calcining schedule for La_2O_3

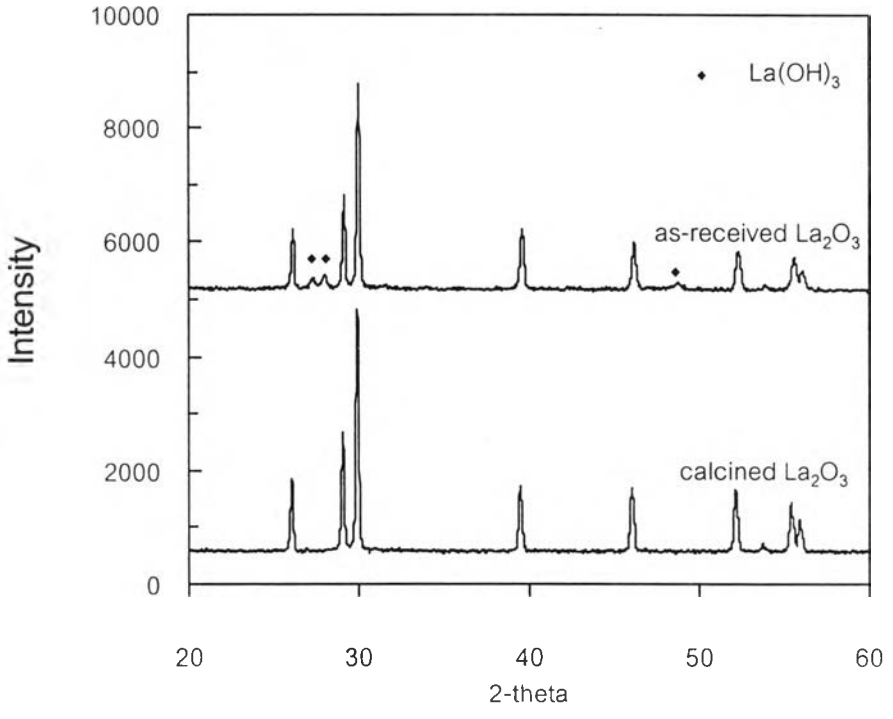

Fig.4.4 XRD patterns of as-received La_2O_3 and calcined La_2O_3 powder

4.2 Determination of calcining temperature for $La_{0.84}Sr_{0.16}Mn_{1-x}B_xO_3$ (B = Co or Fe)

Similar to La_2O_3, the calcining temperatures of all compositions were determined by DTA. After mixing of raw materials, the dried powder of LSM, LSMC4 and LSMF4 was characterized by means of thermal analysis. LSMC4 and LSMF4 were selected as the representatives of LSMC2 and LSMF2, respectively. The DTA curves of those compositions were shown in Fig.4.5. The reaction peaks of LSMC4 and LSMF4 were similar to that of undoped LSM. The exothermic peaks existed around 225-250°C and the endothermic peaks appeared around 360-370, 510-530 and 850-930°C. The reactions tended to be completed at 1200°C. The intensities of reaction peaks were different in each composition, depending on the amount of powder used to analyze.

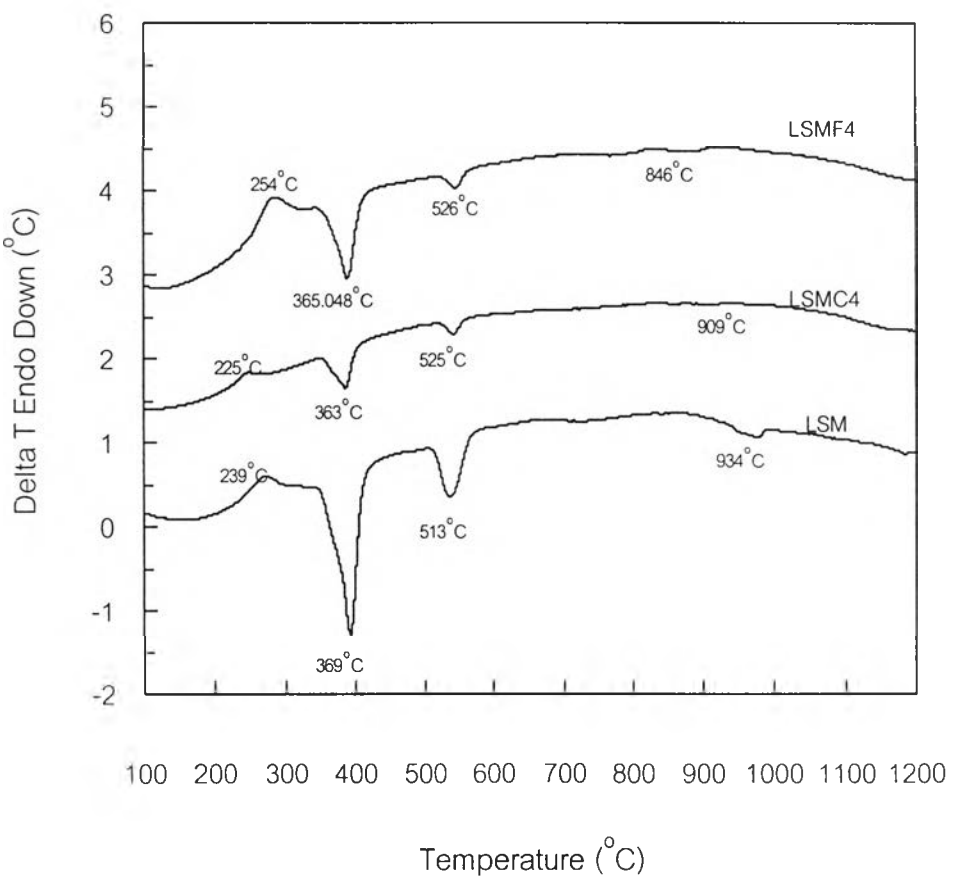

Fig.4.5 DTA traces of LSM, LSMC4 and LSMF4

The powder mixtures of LSM, LSMC2, LSMC4, LSMF2 and LSMF4 were calcined at 1200°C, following the schedule in Fig.4.6. The intermediate soaking was set at the temperatures which the reaction peaks occurred. The long soaking time was performed at the high reaction peaks in order to complete reactions at that temperature. The results of XRD patterns of calcined powder in Fig.4.7 indicated that the pure perovskite phase was obtained; therefore, this calcining condition was suitable for all compositions.

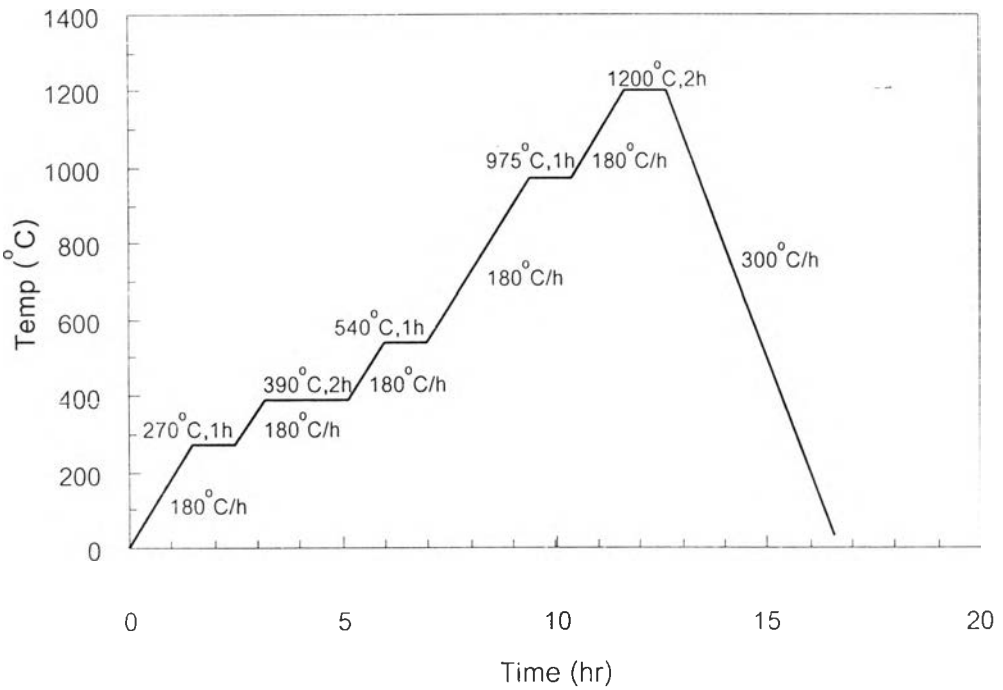

Fig.4.6 Calcining schedule for LSM, LSMC2, LSMC4, LSMF2 and LSMF4

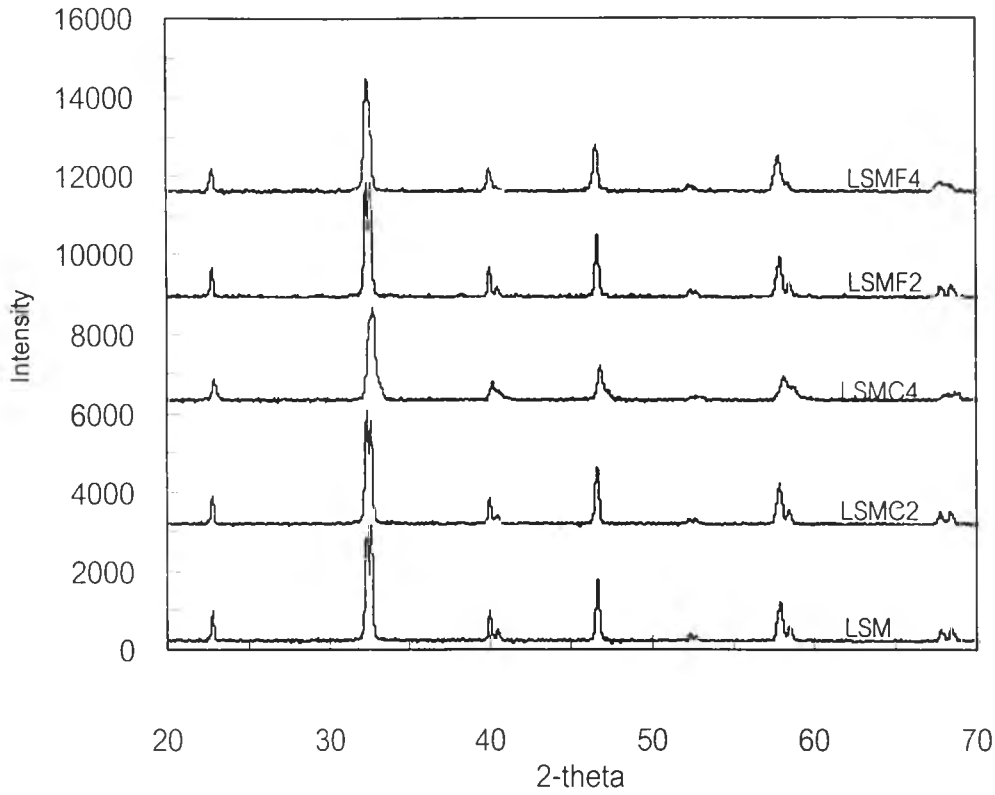

Fig.4.7 XRD patterns of LSM, LSMC2, LSMC4, LSMF2 and LSMF4 powder calcined at 1200°C 2 h

4.3 Effect of dopants on calcined powder

Phases, crystal structures and lattice parameter were conducted by X-ray diffraction. Their results were used to identify the theoretical density of each composition. The calcined powder was mixed with Si standard powder to calibrate the d value. Fig.4.8 showed the XRD patterns of all calcined compositions mixed with Si powder. The Si powder showed the reflections patterns of (111) and (220) 28° and 47° of 2θ. These results indicated that almost all compositions except LSMF4 exhibited a single phase of monoclinic structure corresponding to JCPDS no.40-1100. However, LSMF4 appeared to be orthorhombic structure since only one peak instead of two peaks presented at 32.42° (Appendix B). These results can be concluded that the monoclinic structure could sustain even 40 mol% Co dopant. On the other hand, the monoclinic transformed to orthorhombic

when the Fe content was up to 40 mol%. The calculated unit cell dimensions and x-ray density of all calcined compositions were given in Table 4.1.

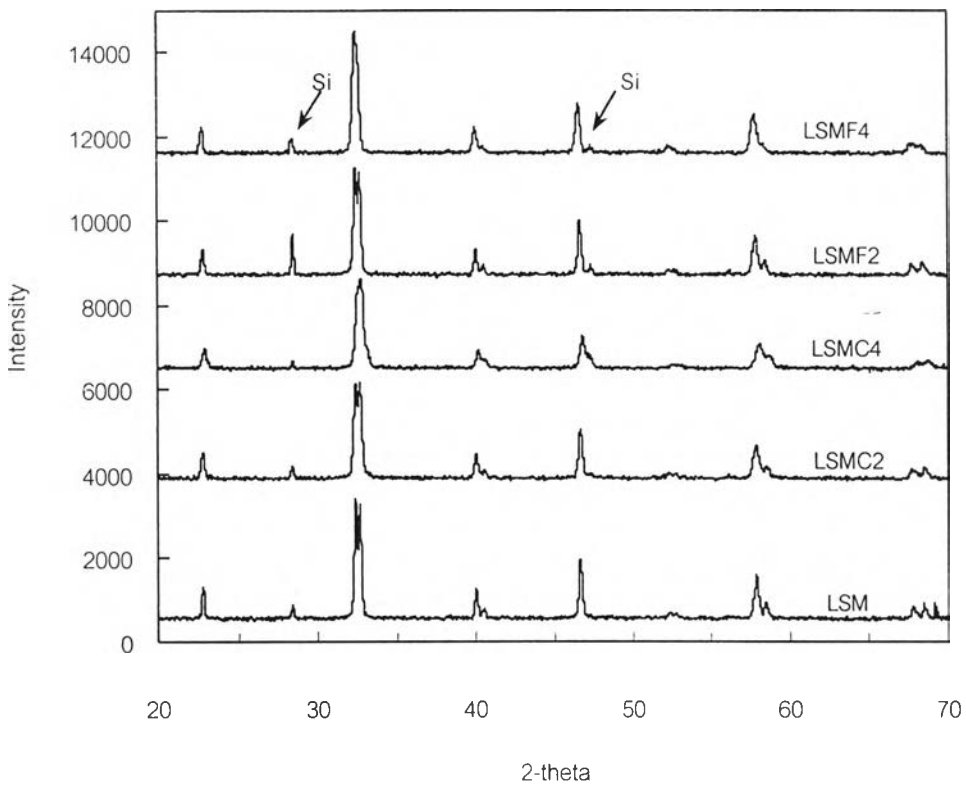

Fig.4.8 XRD patterns of LSM, LSMC2, LSMC4, LSMF2 and LSMF4 powder calcined at 1200°C 2 h and mixed with Si powder

From Table 4.1, it could be seen that as the Co content increased, the unit cell size decreased attributing to a smaller radius of Co ion than that of Mn ion as shown in Table 4.2. Moreover, Co has a higher molecular weight, resulting in an increase of x-ray density.

Table 4.1 The lattice parameters and x-ray density of calcined powders at 1200°C

Composition	Crystal structure	Lattice parameters				Cell volume ($Å^3$)	X-ray Density ($g\ cm^{-3}$)
		a (Å)	b (Å)	C (Å)	β		
LSM	Monoclinic	5.491	5.529	7.784	90.586	236.308	6.57
LSMC2	Monoclinic	5.480	5.523	7.780	90.488	235.461	6.62
LSMC4	Monoclinic	5.479	5.509	7.772	90.001	234.589	6.66
LSMF2	Monoclinic	5.480	5.536	7.788	90.671	236.250	6.58
LSMF4	Orthorhombic	5.535	5.529	7.796	-	238.581	6.52

Table 4.2 Ionic radii of cations[23]

Ions	Ionic radius (Å)
Mn^{3+}	0.58
Mn^{4+}	0.53
Co^{2+}	0.58
Co^{3+}	0.53

In general, doping $LaMnO_3$ with a lower valence cation such as Sr substituted on lanthanum site results in charge transition of Mn^{3+} into Mn^{4+}. The amount of charge compensation depends on the content of Sr dopant. Since 16 mol% of Sr were used through this research, the expected formula was $La_{0.84}Sr_{0.16}Mn^{3+}_{0.84}Mn^{4+}_{0.16}O_3$ (LSM).

The substitution of Co_3O_4, mixed oxide of Co^{2+} and Co^{3+}, in LSM, which decreased the unit cell volume, can be possibly explained in 4 cases

1. Substitution of Co^{2+} in Mn^{3+}

Co^{2+} and Mn^{3+} have the same cation sizes; however, the charge neutrality is compensated by the change in valency state of Mn^{3+} to Mn^{4+}. The smaller size of Mn^{4+} brought about the unit cell contraction.

2. Substitution of Co^{2+} in Mn^{4+}

Although Co^{2+} has a larger size than Mn^{4+}, the substitution of each Co^{2+} into Mn^{4+} can transfrom two ions of Mn^{3+} into Mn^{4+} with the same amount for the charge compensation. Thus, the unit cell size decreases.

3. Substitution of Co^{3+} in Mn^{3+}

In spite of the same charge of 3+, the size of Co^{3+} is smaller than that of Mn^{3} , affecting the unit cell reduction.

4. Substitution of Co^{3+} in Mn^{4+}

Both cations have the same size but the charge neutrality is required. Thus, if each of Co^{3+} replaces each of Mn^{4+}, there should have a transformation of Mn^{3+} to Mn^{4+}, resulting in a decrease of the unit cell volume.

4.4 Effect of dopants on properties of specimens sintered at 1450°C for 2 hours

4.4.1 Phase Analysis

The pellet specimens prepared from perovskite oxide powder were sintered at 1450°C for 2 hours. Then the phases of sintered specimens were determined by XRD to ensure that the single phase was obtained. The analysis was performed at the surface of pellets. XRD results of all compositions were shown in Fig.4.9.

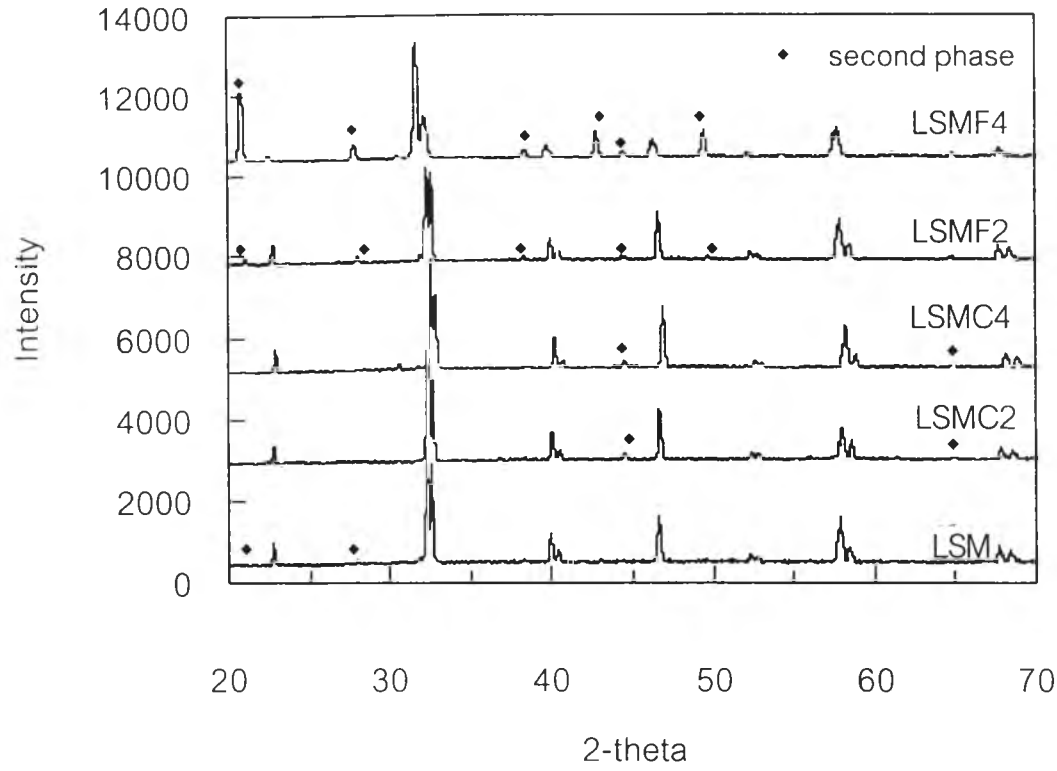

Fig.4.9 XRD patterns of LSM, LSMC2, LSMC4, LSMF2 and LSMF4 pellets sintered at 1450°C 2 h

It was evident that there were some extra peaks appeared on the XRD patterns for all compostions. Those peaks in LSM were observed at 2θ 21° and 28°. But the extra peaks of LSMC2 and LSMC4 occurred at 2θ 44.5° and 65°. These peaks could be due to the presence of the second phases. However, these peaks could not be satisfactorily matched with any of the known crystalline phases in the La-Sr-Mn-Co system and this was beyond in this study. Small amount of second phases in LSM, LSMC2 and LSMC4 might be caused by an inappropriate firing condition such as maximum temperature or soaking time which could induce the separation of second phases.

It was clearly seen that XRD patterns of LSMF2 showed many other peaks beside those of undoped LSM. The amount of second phases became larger in LSMF4,

determined by the relative intensity of peaks. This suggested that doping Fe up to 40 mol% limited the solubility of Fe in LSM at 1450°C.

4.4.2 Density

By Archimedes method, the bulk density of all sintered specimens were measured and its result was shown in Table 4.3.

Table 4.3 Bulk density of specimens sintered at 1450°C 2 h

Composition	Bulk density (g cm^{-3})
LSM	6.37
LSMC2	6.40
LSMC4	6.60
LSMF2	6.21
LSMF4	6.23

From XRD results, there were second phases in sintered specimens of all compositions. Thus, the x-ray density could not be identified. However, Table 4.3 showed that the bulk densities of all compositions were less than x-ray density as given in Table 4.1. Regardless of the small amount of second phases in LSM, LSMC2 and LSMC4, the bulk density tended to increase as Co content increased, attributing to a decrease of lattice parameter associated with higher molecular weight of Co as discussed in 4.3. This result corresponded to the theoretical density result. On the contrary to Co doping, the x-ray density decreased as Fe content increased as appeared in Table 4.1. However, the experimental result was different since other phases existed after sintering at 1450°C, as detected by XRD.

4.4.3 Electrical conductivity

DC four-point method was used to measure the electrical conductivity of these cathode materials. The electrical conductivity of LSM based materials occurs via a small polaron hopping, which is thermally activated process. Therefore, the electrical conductivity (σ) depends upon the temperature measurements and can be expressed by Arrhenius equation as follows:

$$\sigma = \frac{A}{T} \exp\left(-\frac{E_a}{RT}\right) \qquad (4.1)$$

where T is the absolute temperature and R is the gas constant. E_a is an activation energy (kJ mol^{-1}) required for a small polaron hopping process. A is the pre-exponential factor, which is constant. E_a is obtained from the slope of Arrhenius plot between $\frac{1}{T}$ vs log (σT) on the x and y-axis, respectively.

In this study, the following effects on the electrical conductivity were examined.

a) Effect of dopant (Co and Fe)

b) Effect of gold electrode

c) Effect of atmosphere

a) Effect of dopant

The electrical conductivity of rectangular bars sintered at 1450°C for 2 hours was measured as a function of temperature in air. Fired on gold electrode was applied on the rectangular bar for electrical contact before measurement.

The results of the temperature dependence on the conductivity of sintered LSM, LSMC2, LSMC4, LSMF2 and LSMF4 were illustrated in Fig.4.10. The points at slope change defined by phase transitions were not observed for both undoped and doped LSM. For this research, undoped LSM exhibited the highest conductivity for the whole range of

measurement temperature and approached 97 S cm^{-1} at 900°C. Unexpectedly, an addition of 20 mol% Co into LSM decreased its conductivity. Nevertheless, with 40 mol% the conductivity at high temperature inceased. These results could be explained by electron-hole charge compensation. The conductivity of LSM occurred by hole-hopping conduction but the conductivity of LSC (Lanthanum Strontium Cobaltite) was due to electrons from oxygen vacancies. The compensation between electrons and holes could reduce charge carriers in 20 mol% Co doped LSM, corresponding to the decrease of conductivity. An increase of Co content raised the number of electrons. With 40 mol% Co the number of electrons dominated and the conductivity shifted upward.

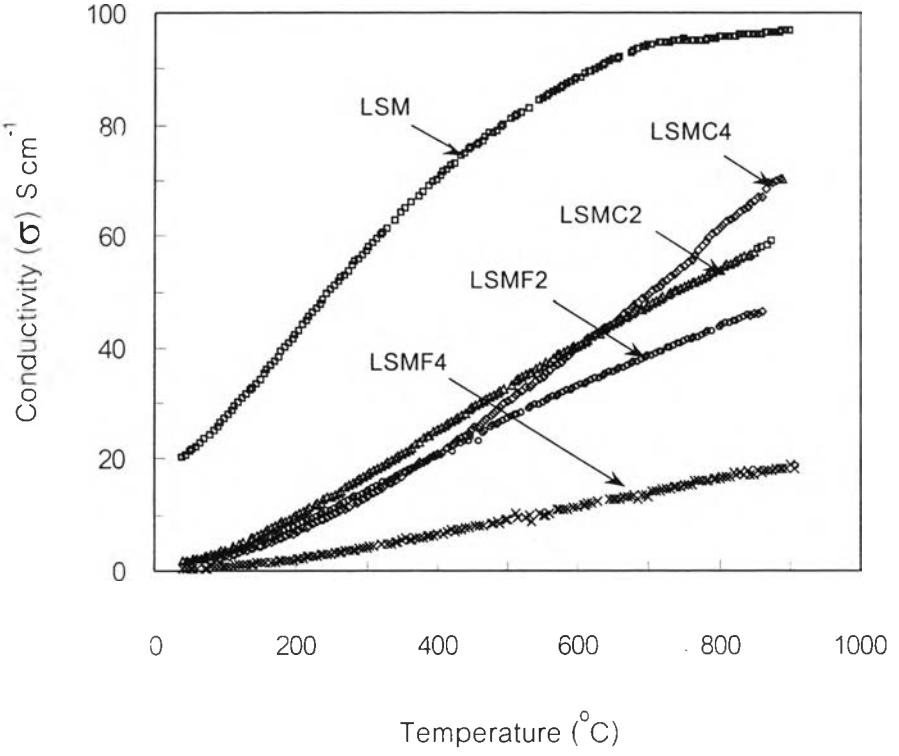

Fig.4.10 Conductivity vs temperature plot of all compositions

sintered at 1450°C 2 h

As Fe content increased, the conductivity decreased as presented in Fig.4.10. The reason for this may be because not only Fe^{3+} itself could not accept hole but also the amount of Mn^{3+} decreased as compared to the base composition. Therefore, the transitions of Mn^{3+} to Mn^{4+} decreased, corresponding to the lower conductivity. In addition, the low conductivity of Fe-doped LSM might be attributed to the presence of second phases as shown in XRD results in Fig.4.9.

The plots of log (σT) and $\frac{1}{T}$ of all compositions were illustrated in Fig.4.11 and Fig.4.12. The electrical conductivities at 1000°C ($\sigma_{1000^{\circ}C}$) and the activation energy (E_a) determined from the slope of each composition were calculated and shown in Table 4.4.

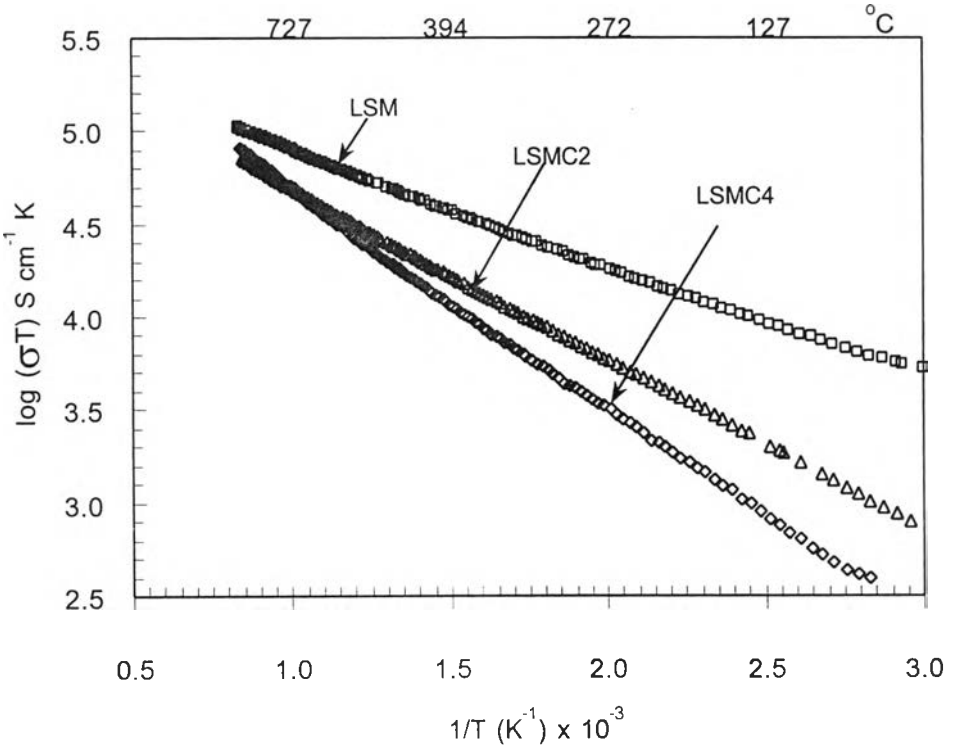

Fig.4.11 Electrical conductivity vs reciprocal temperature of LSM, LSMC2 and LSMC4 sintered at 1450°C 2 h

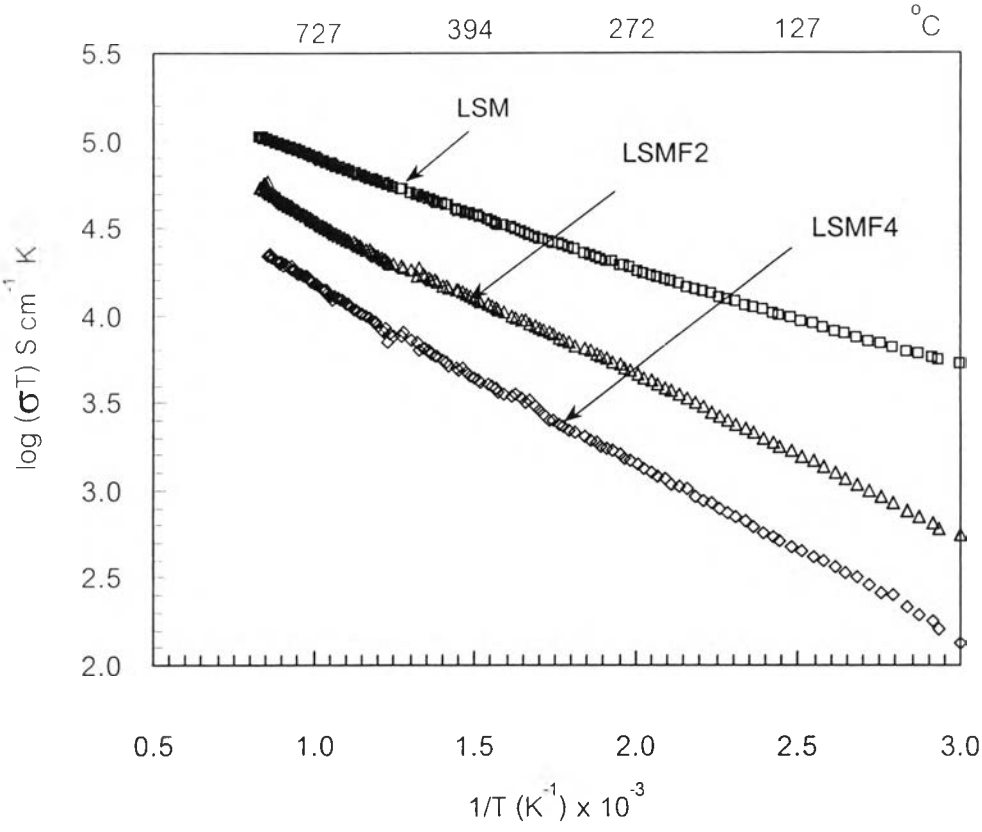

Fig.4.12 Electrical conductivity vs reciprocal temperature of LSM, LSMF2 and LSMF4 sintered at 1450°C 2 h

Table 4.4 Calculated $\sigma_{1000^\circ C}$ and E_a of specimens sintered at 1450°C 2 h

Composition	$\sigma_{1000^\circ C}$ (S cm^{-1})	E_a (kJ mol^{-1})
LSM	99.33	11.61
LSMC2	61.55	17.98
LSMC4	77.33	23.69
LSMF2	59.20	17.38
LSMF4	19.77	19.77

Undoped LSM had the highest $\sigma_{1000^\circ C}$ of 99.33 S cm^{-1}. This value was less than that reported by other researchers for the same composition (170[11] and 133[12] S cm^{-1}) The possible reason for that may be because of the presence of second phase and the

difference in preparation condition such as synthesis method and firing condition. The activation energy for conduction, given in Table 4.4, increased as Co content increased. The activation energy of undoped LSM was 11.61 kJ mol^{-1}, which was close to that of other reports (10.70[11], 9.60[12] kJ mol^{-1}). Similarly, the activation energy appeared to increase with Fe content. This implied that the conductivity of Co or Fe doped composition was much lower than that of undoped LSM.

b) Effect of gold electrode

For electrical conductivity measurement, applying electrode onto the surface of specimen is normally required in order to provide not only good electrical contact but also an increase of measurement area. Since LSM material itself was used as an electrode for fuel cell; therefore, it is worth to study the electrical conductivity without applying gold electrode. Undoped LSM and LSMC4 specimens sintered at 1450°C for 2 hours were selected in this study. Both of these compositions with and without gold on the same specimens were characterized by dc four-point measurement. The results of conductivity as a function of temperature of LSMC4 were illustrated in Fig.4.13. The $\sigma_{1000^\circ C}$ and E_a of LSM and LSMC4 were calculated and shown in Table 4.5.

As seen in Fig.4.13, LSMC4 without gold electrode exhibited lower conductivity at low temperature an higher conductivity at high temperature. The reason for this would be that gold, a metallic conductor, gives a higher resistivity as temperature is raised. This may influence on the conductivity of both cathode materials. The results from Table 4.5 suggested that gold electrode unaffected on the activation energy of compositions. The $\sigma_{1000^\circ C}$ of specimen without gold electrode for both LSM and LSMC4 was higher than that of the same specimen with gold electrode. Without gold electrode applying on specimen, the $\sigma_{1000^\circ C}$ of LSM ($La_{0.84}Sr_{0.16}MnO_3$) approached 165.34 S cm^{-1}. This result was in good agreement to that reported by Mackor et al.[11] (170 S cm^{-1}) and Kertesz et al.[12] (190 S cm^{-1}). It could be concluded that the electrical conductivity of LSM material can be obtained directly using the specimen without gold electrode.

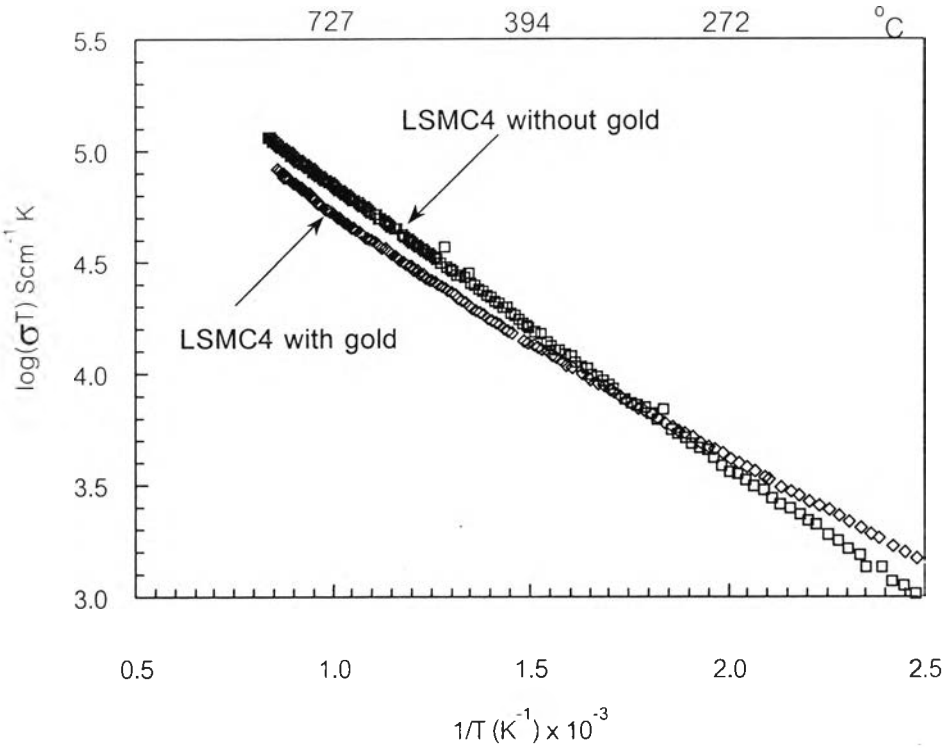

Fig.4.13 Electrical conductivity vs reciprocal temperature of LSMC4 sintered at 1450°C 2 h with and without gold electrode

Table 4.5 Calculated $\sigma_{1000^\circ C}$ and E_a for LSM and LSMC4 sintered at 1450°C 2 h with and without gold electrode

Calculated value	Composition			
	LSM		LSMC4	
	With gold	Without gold	With gold	Without gold
$\sigma_{1000^\circ C}$ (S cm^{-1})	99.33	165.34	77.33	102.79
E_a (kJ mol^{-1})	11.61	11.64	23.69	24.22

b) Effect of atmosphere

Nonstoichiometry in oxide materials, in general, consists of two types of defect structure, oxygen deficiency or metal deficiency, depending upon the partial pressure of oxygen. As oxygen partial pressure increases, either metal deficiency or excess oxygen possible occurs. Since the structure of $LaMnO_3$ is perovskite which is close-packed, only metal deficiency is considered in this composition and its derivatives. Since Sr-doped $LaMnO_3$ ($LaMnO_{3+\delta}$) tended to have more cation vacancies as oxygen partial pressure increased, inducing more small polaron hopping conduction. Thus, atmosphere dependence of electrical conductivity of LSM was studied. The electrical conductivity of LSM sintered at 1450°C for 2 hours was measured in air and being compared to that measured within flowing oxygen condition. The Arrhenius plots were shown in Fig.4.14. Calculated $\sigma_{1000^\circ C}$ and E_a were illustrated in Table 4.6.

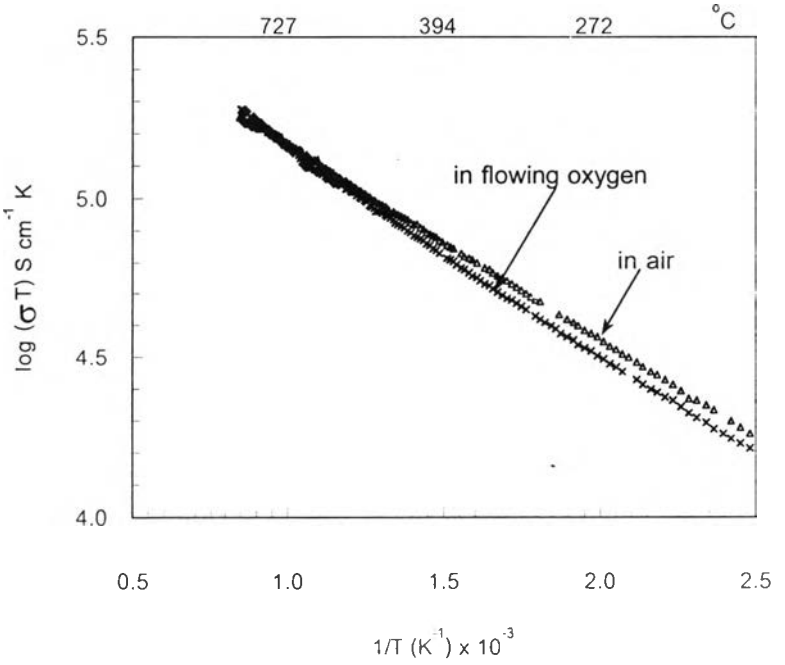

Fig.4.14 Electrical conductivity vs reciprocal temperature of LSM in air and flowing oxygen

Table 4.6 Calculated $\sigma_{1000^{\circ}C}$ and E_a of LSM measured in air and flowing O_2

Measurement Condition	$\sigma_{1000^{\circ}C}$ (S cm^{-1})	E_a (kJ mol^{-1})
In air	165.34	11.64
Flowing O_2	159.33	13.16

It was evident that the electrical conductivity of LSM in flowing oxygen was slightly less than that measured in air, as shown in Fig.4.14. However, at above 500°C, the electrical conductivity measured in both conditions was not different. The $\sigma_{1000^{\circ}C}$ of LSM measured in flowing oxygen was calculated. Its value was slightly lower than that measured in air. Thus, the measurement in flowing oxygen did not have an effect on the electrical conductivity of LSM. This result was in good agreement to other reports[1,18,24] that Sr-doped $LaMnO_3$ ($La_{1-x}Sr_xMnO_{3+\delta}$) was almost independent of oxygen excess content (δ).

4.4.4 Microstructure

The microstructures of the specimens sintered at 1450°C were examined by scanning electron microscope (SEM). Fig.4.15-4.19 showed the SEM micrographs of all polished samples. Intergranular and intragranular pores were observed in all compositions. The formation of pores in Sr-doped $LaMnO_3$ has been reported[10]. Aruna et al.[10] suggested that the dominating effect in sintering of this material was cationic diffusion, which depended on powder morphology, the difference in ionic radii between lanthanum and strontium and the increasing of strontium content.

The average grain size of LSM was about 15-20 microns. As Co content increased, the average grain size did not changed for 20 mol%Co (LSMC2); however, it decreased significantly to about 5-10 microns for 40 mol%Co (LSMC4). On the contrary, the average grain size increased as Fe content increased. It was remarkable that there

were a larger amount of second phases appeared both inside grain and the grain boundary of LSMF2 and LSMF4.

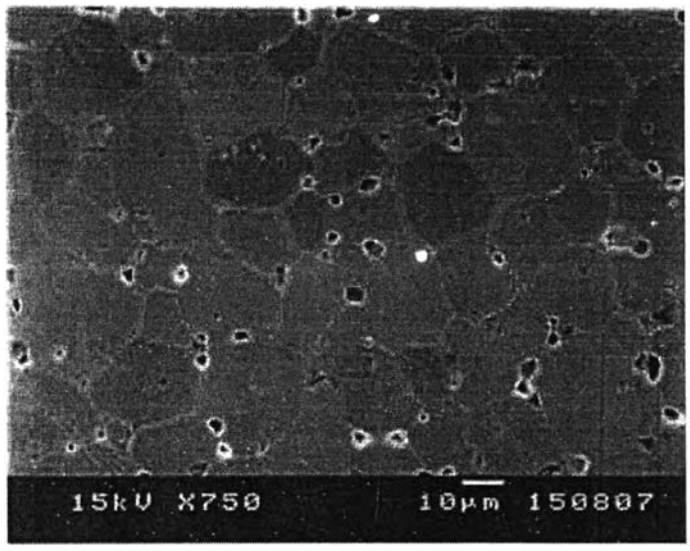

Fig.4.15 SEM micrograph of LSM sintered at 1450°C 2 h

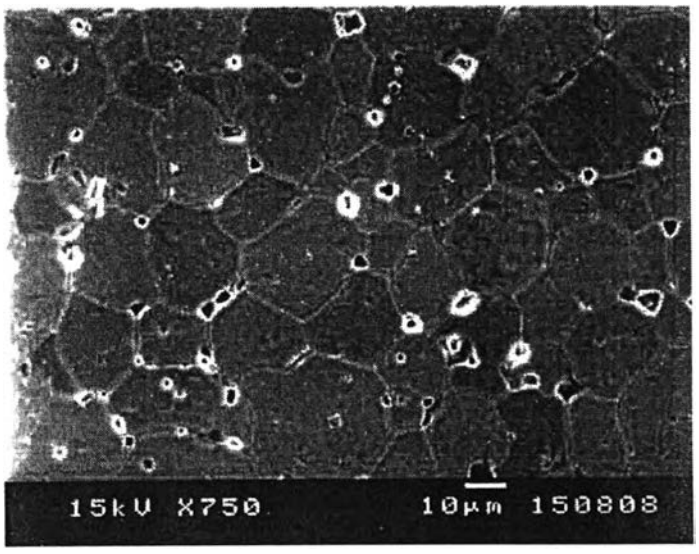

Fig.4.16 SEM micrograph of LSMC2 sintered at 1450°C 2 h

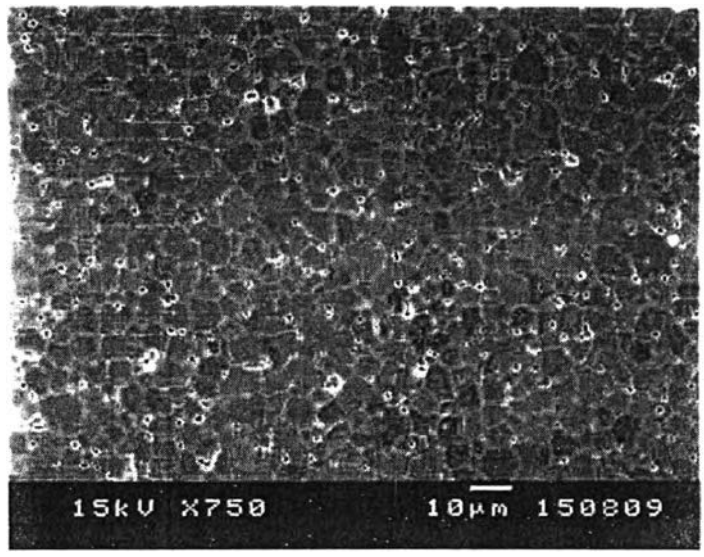

Fig.4.17 SEM micrograph of LSMC4 sintered at 1450°C 2 h

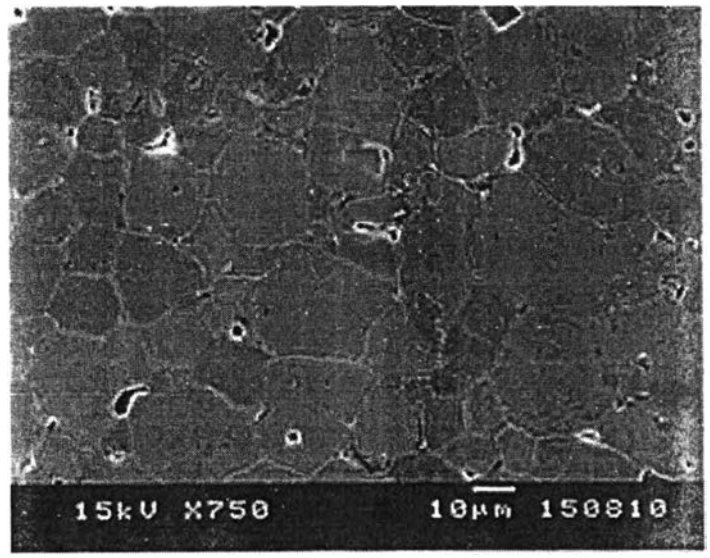

Fig.4.18 SEM micrograph of LSMF2 sintered at 1450°C 2 h

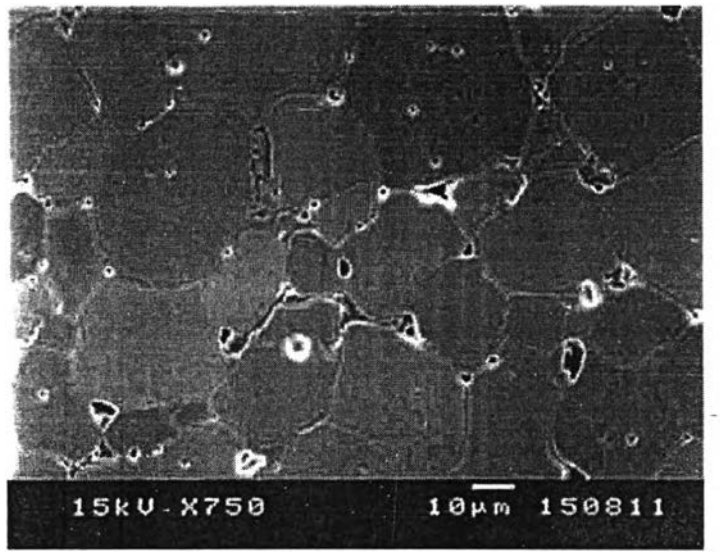

Fig.4.19 SEM micrograph of LSMF4 sintered at 1450°C 2 h

4.4.5 Thermal expansion coefficient

A dilatometer was used to measure the thermal expansion coefficient of sintered specimens. All compositions exhibited positive linear thermal expansion coefficient from room temperature to 900°C. The linear thermal expansion coefficient of LSM was shown in Fig.4.20. Thus, it was confirmed that there was no phase transition occurred during thermal cycling. The values of thermal expansion coefficient, from 100°C to 900°C of all compositions, were calculated and listed in Table 4.7.

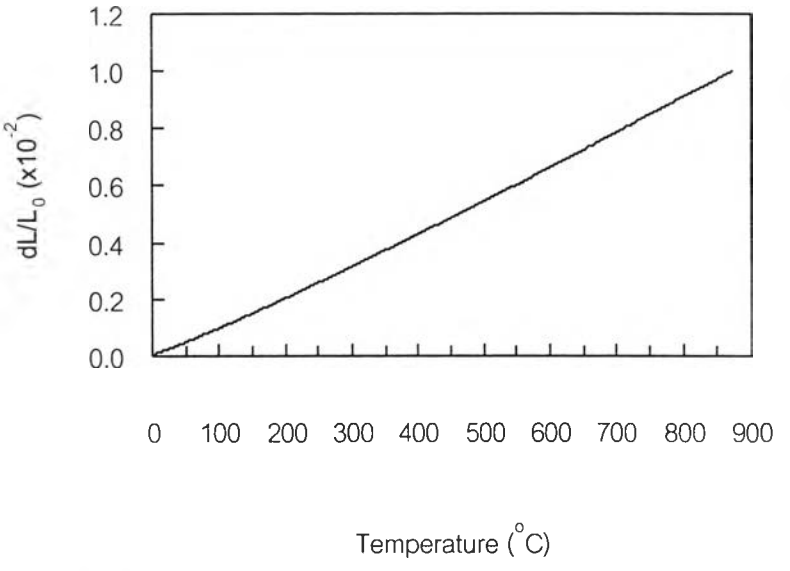

Fig.4.20 Linear thermal expansion coefficient of LSM sintered at 1450°C 2 h

Table 4.7 Thermal expansion coefficient (TEC) specimens sintered at 1450°C 2 h

Composition	TEC (100-900°C) (K^{-1}) X10^{-6}
LSM	11.62
LSMC2	11.69
LSMC4	13.63
LSMF2	11.58
LSMF4	11.55

The measured TEC of undoped LSM or $La_{0.84}Sr_{0.16}MnO_3$ in this experiment was slightly different from other reports (12.63[10] and 11.9[11]). The value of 11.62×10^{-6} K^{-1} was close to that of YSZ (10.5×10^{-6} K^{-1})[7]. The TEC increased as Co content increased. The value of LSMC4 approached 13.63×10^{-6} K^{-1}, which was higher than that of YSZ electrolyte. TEC decreased as Fe content increased. However, the decreasing of TEC was insignificant. The TEC measured for all compositions were acceptable for using with YSZ electrolyte, except LSMC4, of which TEC was over 20% different from that of YSZ[11]. However, the additional properties such as electrical conductivity and chemical stability must be considered for suitable cathode materials.

4.5 Effect of sintering temperature on the properties of sintered specimens

In order to reduce the formation of second phases in specimens sintered at 1450°C for 2 hours, sintering at other temperatures was studied. Two sintering conditions were proposed for LSM and LSMC4 as selected compositions in this work.

1. Sintering at 1400°C for 2 hours

This sintering condition was set out under the assumption that sintering temperature at 1450°C may be too high, corresponding to the decomposition or separation of second phases as observed in the XRD results. None or less second phase was expected in sintering at lower temperature for the same soaking time.

2. Sintering at 1470°C for 1 hour

If the soaking time has an effect on the appearance of second phases, sintering with the shorter soaking time should reduce or eliminate the second phases. However, it may bring down the density of specimen. Thus, sintering at higher temperature and with shorter soaking time were required and performed in order to prevent the formation of second phase and promote densification, respectively.

After sintering at 1400°C for 2 hours and at 1470°C for 1 hour, the sintered specimens were characterized by XRD in order to determine the traces of second phases and compared to that sintered at 1450°C for 2 hours. The results of XRD patterns in Fig.4.21 showed the phases occurred in LSM specimens sintered in three

conditions. The second phases observed in LSM specimens which were sintered at each condition were similar to one anotner. In addition, their relative intensities of second phase were also not different. LSMC4 showed the similar results of XRD, as shown in Fig.4.22. The measurement density was performed in all specimens sintered at 1450°C for 2 hours and 1470°C for 1 hour and summarized in Table 4.8.

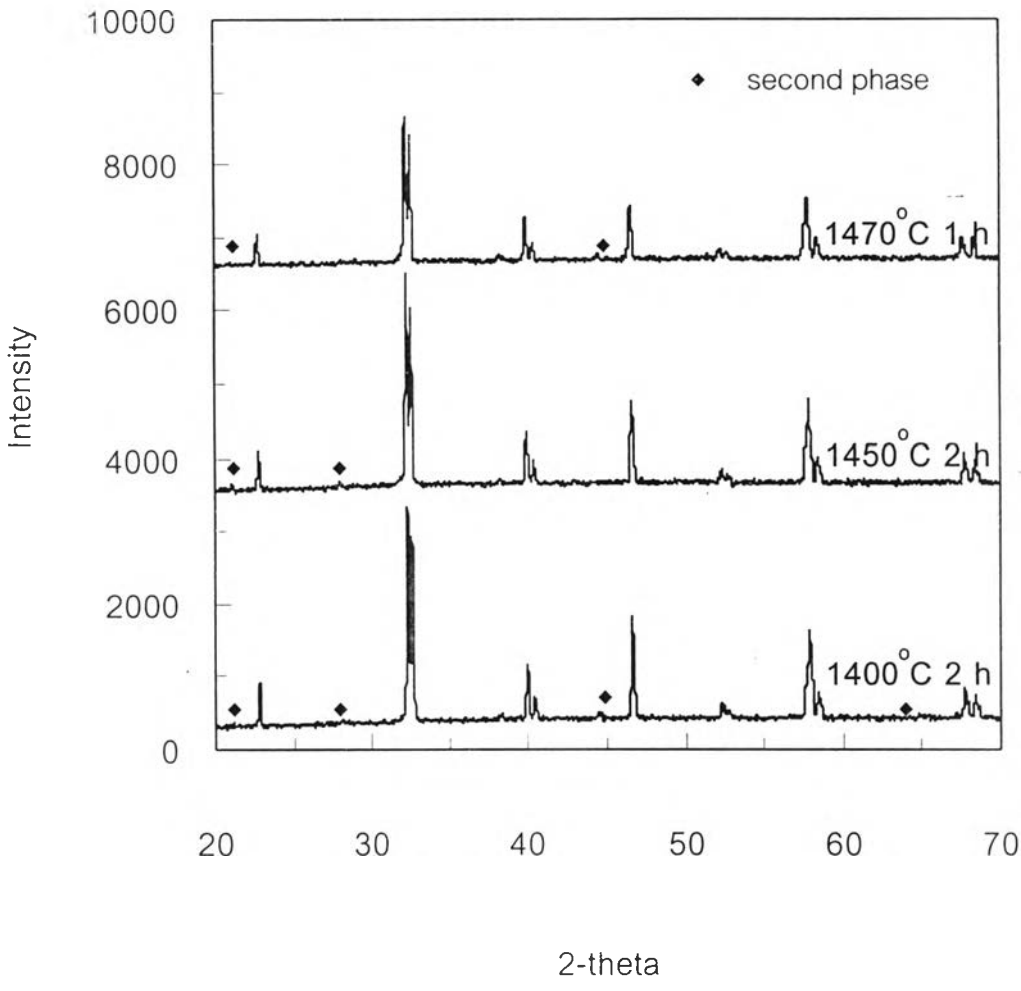

Fig.4.21 XRD patterns of LSM sintered at different conditions

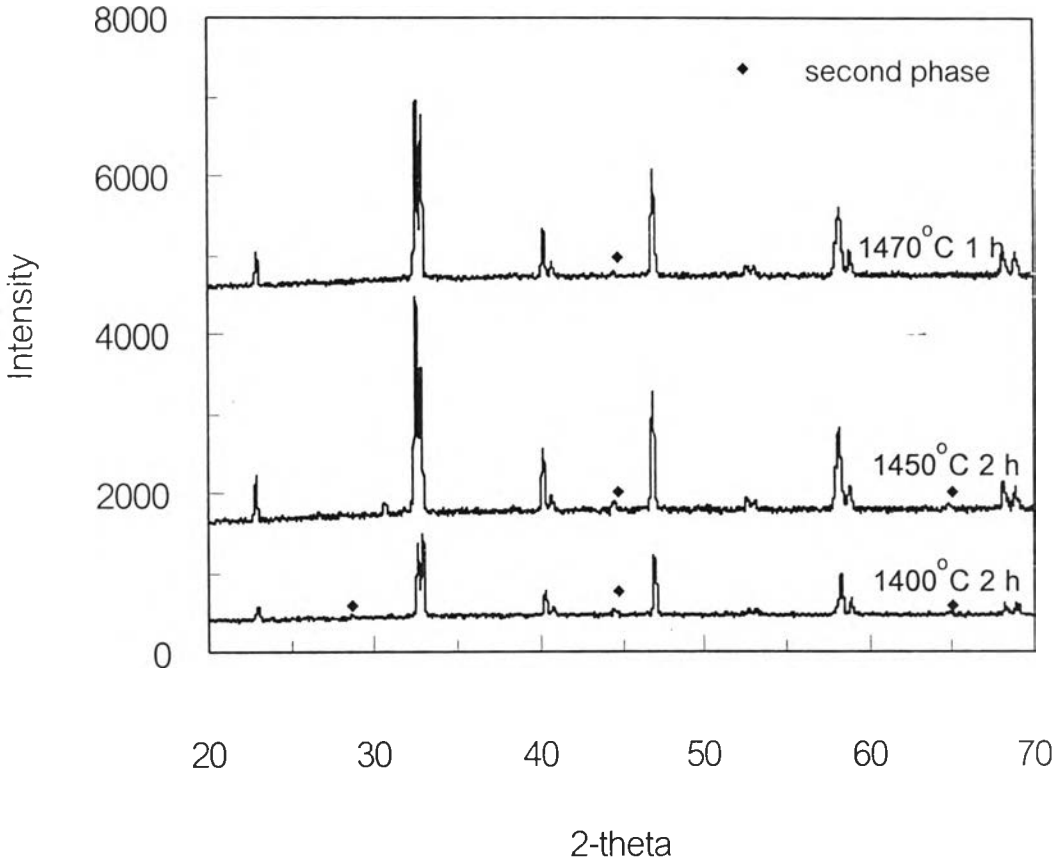

Fig.4.22 XRD patterns of LSMC4 sintered at different conditions

Table 4.8 Density of LSM and LSMC4 at different sintering conditions

Composition	Density at different sintering conditions		
	1400°C 2 hours	1450°C 2 hours	1470°C 1 hour
LSM	6.30	6.37	6.39
LSMC4	6.58	6.60	6.68

The density of specimen increased as sintering temperature increased. It can be concluded that the second phases in sintered specimen occurred at about 1400°C. Sintering at higher temperature with shorter soaking time cannot reduce the formation of second phases. Therefore, sintering at temperature below 1400°C is recommended for LSM. Although it will lower the density, a cathode in fuel cell, generally, must be porous to allow air or oxygen transport through all sites of cathode.